Journal of Controlled Release 343 (2022) 457–468

Contents lists available at ScienceDirect

Journal of Controlled Release

journal homepage: www.elsevier.com/locate/jconrel

Targeted downregulation of HIF-1α for restraining circulating tumor microemboli mediated metastasis

Junjie Du [1], Cong Wang [1], Yijun Chen, Lingyu Zhong, Xuwentai Liu, Lingjing Xue, Ying Zhang, Yanyi Li, Xiaoyu Li, Chunming Tang, Zhigui Su [*], Can Zhang [*]

State Key Laboratory of Natural Medicines, Jiangsu Key Laboratory of Drug Discovery for Metabolic Diseases, Center of Advanced Pharmaceuticals and Biomaterials, China Pharmaceutical University, Nanjing 210009, PR China

ARTICLE INFO

Keywords:
Metastasis
Circulating tumor microemboli
Hypoxia-inducible factor
BAY 87-2243
Neutrophil cyto-pharmaceuticals

ABSTRACT

Tumor metastasis is directly correlated to poor prognosis and high mortality. Circulating tumor cells (CTCs) play a pivotal role in metastatic cascades, of which CTC clusters is highly metastatic compared to single CTCs. Although platelets and neutrophils within the bloodstream could further exacerbate the pro-metastatic effect of single CTCs, the influence of platelets and neutrophils on CTC clusters mediated metastasis remains unclear. In this study, a pro-metastatic complex composed of CTC clusters, platelets and neutrophils, namely circulating tumor microemboli (CTM), was identified *in vivo* among different metastatic tumor, which was demonstrated with highly upregulation of hypoxia-inducible factor-1α (HIF-1α). While knock-out of HIF-1α or therapeutically downregulating of HIF-1α *via* HIF-1α inhibitor (BAY87–2243)-loaded neutrophil cyto-pharmaceuticals (PNEs) could efficiently restrain CTM mediated lung metastasis. The underlying mechanism of metastasis inhibition was attributed to the downregulation of HIF-1α-associated PD-L1, which would enhance immune response for inhibiting metastatic cells. Thus, our work here illustrates that hypoxia was an essential factor in promoting CTM colonization in lung. More importantly, we provide a promising strategy by targeted downregulation of HIF-1α in CTM *via* neutrophil cyto-pharmaceuticals for treatment of CTM mediated metastasis.

1. Introduction

Metastasis remains the major cause of cancer-related death worldwide [1]. Metastasis is the process by which tumor cells shed from the primary sites, spread away by the bloodstream or lymphatic system, and finally metastasize to a specific organ [2,3]. These tumor cells released from the lesion were so called as circulating tumor cells (CTCs), which were found in different modes including single CTCs or CTC clusters [4]. Previous studies reported that the metastatic potential of CTC clusters is 23- to 50-fold increase when compared to single CTCs [5,6]. During circulation, many components in bloodstream or lymphatic system also involved in regulating the CTCs mediated metastasis. It was reported that platelets 'cloaking' on the surface of CTCs would assists CTCs to avoid clearance by natural killer cells [7,8]. Meanwhile, platelets upon contacting with CTCs could secret the chemokines of CXCL5 and CXCL7, which would further recruit the granulocytes such as neutrophils (NEs) to CTCs [9]. In addition, CTCs can 'hijack' NEs to directly form CTCs-neutrophils clusters (CTCs-NEs clusters), endowing CTCs with great proliferative advantage and metastatic potential [10]. Moreover, NEs also facilitate adhesion between CTCs and endothelium, which would promote the extravasation and colonization of CTCs [11]. As we known so far, the studies about interaction between CTCs with platelets or NEs for promoting metastasis mainly focus on single CTCs, but for CTC clusters the interaction on enhancing metastasis remain very limited. In addition, whether CTC clusters simultaneously interact with platelets and NEs (referred to circulating tumor microemboli, CTM) is also unillustrated. Hence, exploration of the mechanism of metastasis induced by CTC clusters with platelets and NEs is clearly of significance, which might offer some fantastic interventional approaches for metastasis therapy.

Notably, CTC clusters were found to undergo hypoxia with high levels of hypoxia-inducible factor-1α (HIF-1α) expression [12], which was the master hypoxia regulatory transcription and closely correlated with metastasis progression [13,14]. It has been confirmed that HIF-1α

* Corresponding authors.
E-mail addresses: zhiguisu707@cpu.edu.cn (Z. Su), zhangcan@cpu.edu.cn (C. Zhang).
[1] Authors contributed equally to this work.

https://doi.org/10.1016/j.jconrel.2022.01.051
Received 27 September 2021; Received in revised form 31 January 2022; Accepted 31 January 2022
Available online 3 February 2022

is also closely related to the expression of adhesion molecules [15], which might facilitate the formation of CTM consisted of CTC clusters, platelets and NEs. Moreover, previous studies reported that platelets adhesion can cause NF-κB dependent HIF-1α transcriptional activation in CTCs [16], and reactive oxygen species produced by neutrophil respiratory bursts can effectively inhibit the degradation of HIF-1α [17]. The above reports indicated that CTM would still possess high level of HIF-1α expression with hypoxia status. Moreover, immune checkpoint molecules such as PD-L1 are downstream target genes of HIF-1α [18], which would help the immune escape of CTCs. But the expression of PD-L1 in CTM is poorly understood. Hence, we speculate that suppression of HIF-1α in CTM may alleviate hypoxia, which would result in reducing the expression of PD-L1 for inhibition of immune escape, finally impeding CTM promoting metastasis.

As a proof-of-principle demonstration, we first proved the CTM composed of CTC clusters, platelets and NEs as novel metastatic entity in tumor metastasis, with overexpressed HIF-1α and possessing robust metastatic potential *via* PD-L1 mediated immune escape. Next, based on the chemotaxis of neutrophils to CTM, we exploited the neutrophil cyto-pharmaceuticals (PNEs) by internalizing HIF-1α inhibitor (BAY 87–2243) [19] loaded acetylated-dextran nanoparticles (BAY/NP) for targeted inhibition of HIF-1α in CTM, and further illustrated the underlying interventional mechanism of PNEs on CTM mediated metastasis (Fig. 1). Our work would confirm that CTM composed of CTC clusters, platelets and NEs held great potential in promoting tumor metastasis, while targeted downregulation of HIF-1α in CTM may provide a novel strategy against tumor metastasis through inhibiting immune escape.

2. Materials and methods

2.1. Materials

The Ac-DEX was synthesized by Liu's group [20], and ditetradecyl lysylglutamate (TA_2-Glu-Lys, TA_2GL) and BAY 87–2243 were synthesized by our group. Other reagents such as the antibodies for PD-L1 (CD274 Monoclonal Antibody, 17–5982-80; thermo), HIF-1α (ab179483; abcam) were purchased from the indicated suppliers.

2.2. Animals

Female BALB/c mice (20–22 g) and male C57BL/6 mice (20–22 g) were purchased from Comparative Medicine Center of Yangzhou University and maintained under specific-pathogen-free conditions. Mice were allocated randomly to each group. All procedures were approved by the Animal Ethics Committee of China Pharmaceutical University and were conducted in compliance with the Guide for Care and Use of Laboratory Animals.

2.3. Cell culture

4 T1 cells were purchased from the Cell Bank of Chinese Academy of Science (Shanghai, China). B16F10 cells (referred hereafter as B16 cells) were purchased from American Type Culture Collection (ATCC). 4 T1-

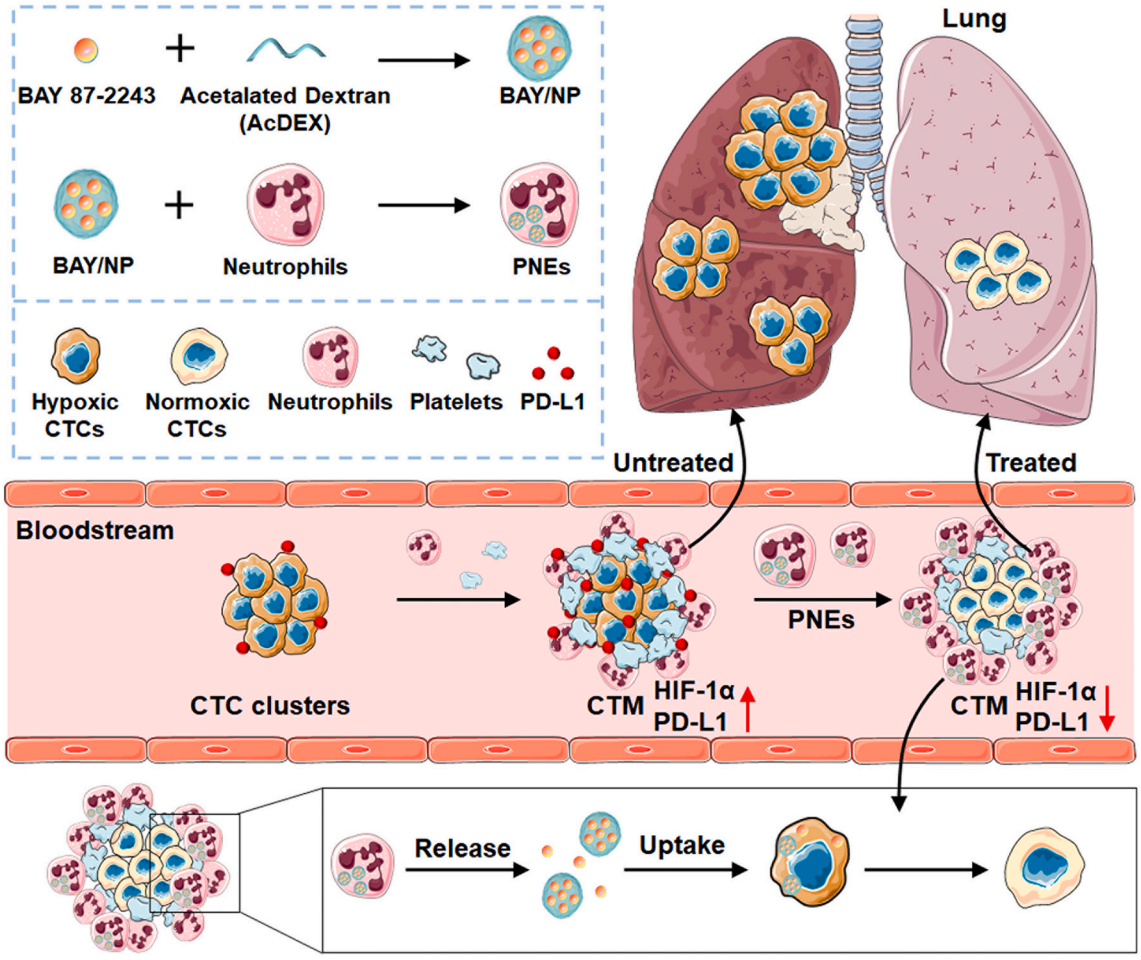

Fig. 1. Schematic illustration of neutrophil cyto-pharmaceuticals targeted downregulation of HIF-1α for restraining circulating tumor microemboli mediated metastasis.

mCherry cells and 4 T1-Luc cells were obtained by transfecting with mCherry and luciferase lentiviral vector respectively and were both maintained in RPMI-1640 medium supplemented with 10% FBS (Gibco, Thermo Fisher Scientific) and 1% penicillin-streptomycin solution. B16F10-mCherry cells (referred hereafter as B16-mCherry cells), B16F10-Luc cells (referred hereafter as B16-Luc cells) all cultured in high glucose DMEM medium supplemented with 10% FBS and 1% penicillin-streptomycin solution. 4 T1 HIF-1α knock down cells ($4T1^{HIF\text{-}1\alpha\text{-}KD}$) were generated as previously reported. For 4 T1-mCherry, 4 T1-Luc, B16-mCherry, B16-Luc cells culture, puromycin (4 μg/mL) was added in the media. All cells were cultured in a humidified incubator with 5% CO_2 at 37 °C and routinely tested for mycoplasma contamination.

2.4. Murine peripheral platelets isolation

Peripheral blood was freshly drawn from anaesthetized BALB/c or C57BL/6 mice *via* the retroorbital plexus. Each 500 μL blood was collected in 100 μL anticoagulant solution (113 mM sodium citrate dihydrate, 137 mM glucose, pH 6.4) and proceeded within 30 min. The blood was firstly centrifuged at 200 *g* for 6 min at room temperature to obtain semi-purified platelet-rich plasma (PRP). The resulting PRP was then centrifuged at 200 *g* for another 6 min to obtain purified PRP. Furthermore, the purified PRP was followed by centrifuging at 800 g for 6 min to prepare platelet pellet, after which the supernatant was discarded and platelets were finally suspended in RPMI-1640 complete medium at a concentration of 1.6×10^8 platelets per 100 μL and proceeded in CTM simulation immediately.

2.5. Murine bone marrow neutrophils isolation

Neutrophils were isolated from bone marrow of healthy BALB/c or C57BL/6 mice by a modified Percoll gradient centrifugation method as previously reported [21]. Briefly, bone marrow unicellular suspension after red blood cells lysed was gently laid onto a Percoll mixture solution consisting of 75%, 65% and 55% (v:v) Percoll in PBS from the bottom up, and followed by centrifugation at 2500 rpm for 30 min at room temperature. The obtained neutrophils were suspended in RPMI-1640 medium at a concentration of 2×10^6 neutrophils per 200 μL and proceeded in CTM models establishment immediately.

2.6. In vivo CTM assays

4 T1-mCherry cells or B16-mCherry cell clusters were directly injected into BALB/c or C57BL/6 mice *via* tail vein at 5×10^5 cells per mouse. Mice were sacrificed 4 h and 16 h post-injection respectively, both time points at which tumor cells remained in the blood circulation before extravasating [16]. Lungs were rinsed with PBS solution repeatedly and fixed in 4% paraformaldehyde for 6 h, followed by gradient dehydration with 15% and 30% sucrose solution overnight. The largest lung lobes were embedded in OCT agents and sectioned into 15 μm thickness slices, fixed in ice-cold acetone for 15 mins and soaked in PBS solution for 10 mins. The lung slices were then blocked in QuickBlock™ Blocking Buffer for Immunol Staining for 10 mins and rinsed with PBS solution repeatedly. The slices at 4 h time points were chosen to verify the existence of CTM *in vivo*, while the ones at 16 h were used to detect the expression of HIF-1α, E-cadherin and Vimentin. The details of immunofluorescence staining were showed in Supporting Information.

2.7. In vitro CTM models establishment

4 T1 cells were seeded in ultra-low attachment plates (3471, Corning) at 2×10^5 cells per well. Each well contained 2 mL RPMI-1640 complete medium. After incubation at 37 °C for 24 h, 4 T1 clusters (4 T1 CL) were obtained. 100 μL aliquots of freshly isolated platelet solution (1.6×10^8) were then added dropwise to each well. After incubation at 37 °C for 2 h without any interference, 4 T1 clusters-Platelets (4 T1 CL-PLTs) were prepared. Afterwards, 200 μL aliquots of freshly isolated neutrophil solution (2×10^6) were added dropwise and incubation for another 16 h to prepare 4 T1 clusters-Platelets-Neutrophils (4 T1 CTM). B16 CTM were simulated under the similar process with platelets and neutrophils both derived from syngeneic C57BL/6 mice. The characteristics of CTM was assayed by immunofluorescence staining and observed by confocal laser scanning microscopy (CLSM). The morphology of CTM was also imaged by scanning electron microscope (SEM). The expression of HIF-1α in CTM was analyzed by western blot and real-time PCR. The downstream genes of HIF-1α including glucose transport 1 (*Glut1*), pyruvate dehydrogenase kinase 1 (*Pdk1*), vascular endothelial growth factor A (*Vegfa*), lactate dehydrogenase A (*Ldha*), growth differentiation factor 15 (*Gdf15*), cyclin G2 (*Ccng2*) and collagen prolyl 4-hydroxylase αsubunit 1 (*P4ha1*) were analyzed by real-time PCR. The details about the RNA extraction method were showed in Supporting Information. cDNA was synthesized using HiScript II Q RT SuperMix for qPCR (R223–01, Vazyme Biotech Co.,ltd). Real-time PCR was performed on a StepOne system using qPCR SYBR Green Master Mix (11203ES08, Yeasen). Primers were listed in Table S1.

2.8. Assessment of metastatic potential of different entities

To assess the metastatic potential of different tumor metastatic entities during tumor metastasis process, female BALB/c mice were intravenously injected with equal amount of different cellular populations *via* tail vein. $4T1^{HIF\text{-}1\alpha\text{-}KD}$ cells and 4 T1 cells were seeded in 6-well plates at 2×10^5 cells per well and cultured for 48 h, and $4T1^{HIF\text{-}1\alpha\text{-}KD}$ single cells ($4T1^{HIF\text{-}1\alpha\text{-}KD}$ SC) and 4 T1 single cells (4 T1 SC) were obtained after 0.25% trypsin digestion. At the same time, $4T1^{HIF\text{-}1\alpha\text{-}KD}$ cells and 4 T1 cells were also seeded in ultra-low attachment plates at 2×10^5 cells per well and cultured for 48 h to prepare $4T1^{HIF\text{-}1\alpha\text{-}KD}$ CL and 4 T1 CL. Additionally, 4 T1 CL with Platelets (4 T1 CL-PLTs), 4 T1 CL with NEs (4 T1 CL-NEs) and 4 T1 CTM were all constructed simultaneously according to the CTM simulation process. Before metastatic models establishment, part of each group was taken out and performed trypsin digestion, then the amount of tumor cells in each group were accurately calculated by flow cytometry. The cellular populations were directly injected into the venous circulation without trypsin digestion (except for $4T1^{HIF\text{-}1\alpha\text{-}KD}$ SC and 4 T1 SC group) at 5×10^5 tumor cells per mouse to establish different metastatic entities groups ($n = 8$). $4T1^{HIF\text{-}1\alpha\text{-}KD}$ cells and 4 T1 cells expressed equivalent luciferase signal determined by IVIS Spectrum (PerkinElmer). To conduct the bioluminescence imaging, mice were intraperitoneally injected with D-Luciferin at a concentration of 150 mg/kg lasting for 10 mins, followed by anaesthetized with 2% isoflurane for 2 mins. Bioluminescence imaging was performed by IVIS Spectrum (PerkinElmer).

2.9. Preparation and characterization of PNEs

The preparation of BAY/NPs (BAY 87–2243 loaded nanoparticles) was performed by a modified oil-in-water (o/w) nanoemulsion solvent evaporation method. In brief, Ac-DEX (25 mg) and BAY (5 mg) were dissolved in 0.25 mL of ethyl acetate and added to 0.75 mL of polyvinyl alcohol (PVA 0486) solution (1% *v*/v in dd-H_2O). The mixture was emulsified by ultrasonication for 30 s in an ice bath using a probe sonicator (10 s pulses intercalated with 2 s intervals, 30% amplitude). The resulting solution was added to 10 mL of polyvinyl alcohol solution (1% v/v in dd-H_2O, pH 8.5 adjusted with 1 mM NaOH). Then, the mixture was evaporated to remove organic solvent under continuous stirring for 4 h. Nanoparticles were isolated by centrifugation at 13,780 *g* for 6 min and washed with dd-H_2O (pH 8.5) for three cycles. Next, the positive lipid TA_2GL (4 mg) was dissolved in 0.25 mL of dd-H_2O (pH 8.5) and mixed with the nanoparticles. After vortex, bath sonication (5 min) and centrifugation at 13,780 *g* for 6 min, the final BAY/NPs were obtained by redispersion in dd-H_2O (pH 8.5). The particle size and zeta potential

were measured by dynamic light scattering and the morphology of BAY/NPs was observed by transmission electron microscopy (TEM). The encapsulation efficiency of BAY/NPs was determined by HPLC.

PNEs (BAY/NP-loaded NEs) were obtained as previously reported [21]. In brief, freshly isolated neutrophils were incubated with BAY/NP at BAY concentration of 60 μg/mL per 10^5 cells for different time at 37 °C, followed by repeated centrifugating and washing with PBS solution for 3 times. PNEs were lysed with SDS cell lysis buffer (Beyotime, China). The cell lysate (50 μL) was mixed with 200 μL of acetonitrile, vortexed for 5 min and centrifuged at 13,780 *g* for 10 min. The supernatant (20 μL) was injected into the HPLC system for quantification.

To further study the uptake of BAY/NP by NEs, fluorescent molecular of coumarin 6 was used to label BAY/NPs (Coumarin 6-BAY/NPs) and then incubated with NEs. The fluorescent signal of Coumarin 6- BAY/NPs in NEs was detected by CLSM. The chemotaxis assays of PNEs were investigated. Simulated CTM were suspended in RPMI-1640 medium without FBS and seeded on the bottom of ultra-low attachment plates. 1×10^6 freshly isolated neutrophils or prepared PNEs were stained with DIO cell membrane green fluorescence probe (1:300, C1038, Beyotime), suspended in RPMI-1640 medium without FBS and added onto the upper Transwell chamber (3 μm, Millipore). After 16 h of chemotaxis, the chamber was removed and the recruited green fluorescence labeled neutrophils were recorded using an inverted fluorescence microscope (FV1100, Olympus) at 12 random fields. The average number of migrated neutrophils or PNEs in each group was counted by Image J software. The detailed groups were as follows: 1) Buffer (serum-free RPMI-1640 medium); 2) PLTs; 3) NEs; 4) 4 T1 CL; 5) 4 T1 CL-PLTs; 6) 4 T1 CL-NEs; 7) 4 T1 CTM.

To study the drug uptake behavior of CTM, Coumarin 6-BAY/NPs was used to construct PNEs (Coumarin 6-PNEs). The simulated 4 T1 CTM were co-stained with PE anti-Mouse CD41 (1:300) and DAPI (1:400) in advance. Then, freshly prepared Coumarin 6-PNEs were co-cultured with 4 T1 CTM continuously at 5% CO_2, 37 °C humidified incubator. At indicated time points, 4 T1 CTM were carefully transferred out from the ultra-low attachment plates, followed by gently washing with PBS solution for twice. Representative images were immediately taken using LSM 880 (Zeiss). Note that each time points represented 4 T1 CTM in each well.

The *in vitro* stability of PNEs was evaluated under different conditions, including the normal physiological condition (RPMI medium), during the process of chemotaxis (formyl-met-leu-phe, fMLP), at the site of inflammation (phorbol myristate acetate, PMA) and CTM microenvironment (conditioned medium of CTM). In brief, 8×10^5 PNEs were seeded in 24-well plates, and then incubated with the RPMI and RPMI containing fMLP (10 nM) and PMA (100 nM) for different periods (0.5, 1, 2, 4, 6 and 8 h). The amounts of BAY in the PNEs and released in the supernatant medium were determined using HPLC. The drug release from BAY/NP with similar condition as described above were also investigated by dialysis method and determined using HPLC.

2.10. In vitro intervention process of PNEs

Simulated 4 T1 CTM were grouped and intervened as followings: 1) 4 T1 CTM control; 2) 4 T1 CTM + BAY; 3) 4 T1 CTM + BAY/NP; 4) 4 T1 CTM + NEs; 5) 4 T1 CTM + PNEs. Each group contains BAY 87–2243 equivalent to 10 μM and the intervention time was 20 h. B16 CTM were treated under the same conditions. The hypoxia status and expression of HIF-1α were evaluated by immunofluorescence staining, western blot and real-time PCR. The downstream genes of HIF-1α, such as *Glut1*, *Vegfa*, *Pdk1, Ldha, Gdf15, Ccng2,* and *P4ha1* was also analyzed by real-time PCR. In addition, the mRNA levels of adhesion molecules of *αv*, *P-selectin*, *β3* and *Icam-1*, as well as the epithelial-mesenchymal transition (EMT) genes *Snail* and *Twist*, were also determined by real-time PCR. The details were showed in Supporting Information.

To detect PD-L1 expression in simulated CTM before or after intervention, CTM were centrifugated and thoroughly separated with 0.25% trypsin solution (Hyclone). After washing, cells were stained with APC anti-mouse PD-L1 (1:300) and incubated at 37 °C for 30 mins. 4 T1 single cells and freshly isolated neutrophils were used as control and gate setting. 1×10^5 4 T1 cells or neutrophils from each sample were recorded (Attune NxT, Thermo). All experiments were repeated for three times.

2.11. Establishment of 4 T1 CTM lung metastasis models, efficacy evaluation and safety evaluation

In vitro simulated 4 T1 CTM were directly intravenously injected at 9×10^5 tumor cells per mouse. Before tumor inoculation, part of 4 T1 CTM were trypsin digested and the number of tumor cells in 4 T1 CTM was quantified using flow cytometry. Mice were randomly divided into 5 groups and blindly selected before injection ($n = 12$ per group). After 4 h, mice were treated according to the following regimens: 1) Saline; 2) free BAY (p.o. 4 mg/kg, BAY dissolved in equal volume mixed solution of polyoxyethylene castor oil and ethanol); 3) BAY/NP (i.v. 1 mg/kg); 4) native neutrophils (i.v. 5×10^6 cells); 5) PNEs (i.v. 5×10^6 cells, equivalent to 1 mg/kg BAY). Mice were administered once every two days for totally 10 times.

For efficacy evaluation, the mice in each group were immediately sacrificed after the last bioluminescence imaging, lungs were harvested for *ex vivo* imaging and average radiance was analyzed ($n = 5$). The lungs were rinsed with PBS solution and photographed with a camera, and the number of metastasis nodules were enumerated and compared with the saline group. Then, lungs were fixed with 4% paraformaldehyde, embedded with paraffin and sectioned into 5 μm thickness slices. The whole lung slices were stained with H&E and scanned with a NanoZoomer 2.0 RS digital pathology scanner (Hamamatsu). The survival periods of mice were monitored after treatment ($n = 7$).

For safety evaluation, the major organs were stained with H&E and representative images were taken at 20 × magnification using a BX53 inverted fluorescence microscope (Olympus). The intestine sections were co-stained with alcian blue and nuclear red, and images were taken at 20 × magnification. Pathological assessment of villus length, crypt depth and number of goblet cells per villus were analyzed with Image J software. The body weights of the mice were monitored during treatment.

2.12. 2.14 statistical analysis

Statistical analyses were performed using the GraphPad Prism 7.0 software. All graphical data were presented as mean ± SEM in at least triplicate. Statistical significance was determined using two-tailed Student's *t*-test or One-way ANOVA, in which *P* values <0.05 were considered statistically significance ($^*P < 0.05$; $^{**}P < 0.01$; $^{***}P < 0.001$; $^{****}P < 0.0001$, respectively). Survival results were analyzed according to a Mantel-Cox curve. Significant differences in survival curves were calculated using the log-rank test.

3. Results and discussion

3.1. CTM was hypoxic both in vivo and in vitro

Metastasis has gradually gained consensus as a complicated multi-component and multi-step process [22]. Circulating tumor microemboli (CTM) is drawing considerable attention, but the underlying pro-metastatic mechanisms need to be further explored. To understand the component and morphological features of CTM *in vivo*, we prepared frozen slices of mice lungs after injection of 4 T1-mCherry or B16-mCherry cell clusters *via* the tail vein. Immunofluorescence staining for platelets and neutrophils markers demonstrated the prevalence of their intimate association with 4 T1-mCherry clusters (4 T1-mCherry CL) (Fig. 2A). In separated-channel regions, we clearly found that 4 T1-mCherry CL were surrounded with platelets and NEs in hierarchical

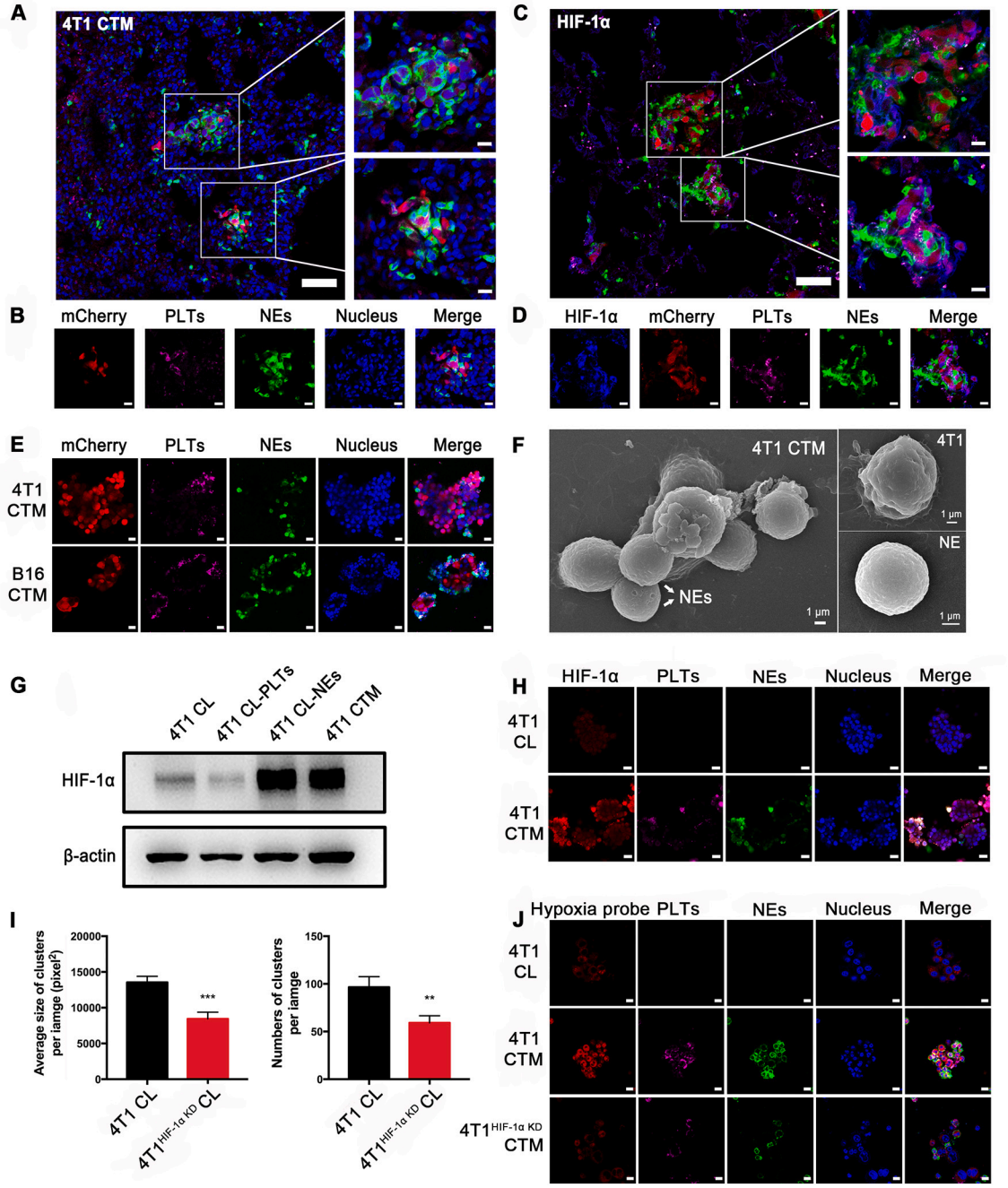

Fig. 2. CTM remained hypoxic both *in vivo* and *in vitro* established models. (A) Representative images of 4 T1 CTM in the lung section slices. 4 T1-mCherry tumor cells (Red) were surrounded by platelets that were labeled with CD41 antibody (Rose red) and neutrophil stained by anti-Ly6G antibody (Green). The nuclei were stained by DAPI (Blue). Scale bar: 50 μm for the left image and 10 μm for the right ones. (B) Separated-channel images of *in vivo* 4 T1 CTM. Scale bar: 10 μm. (C) Representative immunofluorescence images of HIF-1α staining (Blue) in 4 T1 CTM in the lung section slices. Scale bar: 50 μm for the left image and 10 μm for the right ones. (D) Separated-channel images of HIF-1α staining in 4 T1 CTM. Scale bar: 10 μm. I Representative images of *in vitro* established 4 T1 CTM and B16 CTM models. 4 T1-mCherry or B16-mCherry tumor cells (Red) were surrounded by platelets that were labeled with CD41 antibody (Rose red) and neutrophil stained by anti-Ly6G antibody (Green). The nuclei were stained by DAPI (Blue). Scale bar: 20 μm. (F) Representative SEM images of 4 T1 CTM models. Scale bar: 1 μm. (G) The level of HIF-1α in 4 T1 CL, 4 T1 CL-PLTs, 4 T1 CL-Nes, and 4 T1 CTM was examined by western blot. Representative gel electrophoresis bands were shown. (H) Representative immunofluorescence images of HIF-1α staining (Red) in 4 T1 CL and 4 T1 CTM. Scale bar: 20 μm. (I) 4 T1 and $4T1^{HIF\text{-}1\alpha\text{-}KD}$ tumor cells were seeded in ultra-low attachment plates at 2×10^5 cells per well and cultured for 24 h to prepare clusters (CL). Quantitative analysis of average size and number of clusters per image. Scale bar: 200 μm. $N = 13$, $^{**}P < 0.01$, $^{***}P < 0.001$. (J) Representative immunofluorescence images of hypoxia probe staining (Red) in 4 T1 CL, 4 T1 CTM and $4T1^{HIF\text{-}1\alpha\text{-}KD}$ CTM. Scale bar: 10 μm. (For interpretation of the references to colour in this figure legend, the reader is referred to the web version of this article.)

orders to form the 4 T1 CTM, of which platelets served as 'bridges' inside (Fig. 2B). Previous studies revealed that platelets were the first component that interacted with CTCs [23]. This behavior should be due to the high number of platelets in bloodstream and high affinity between platelets with CTCs. Meanwhile, morphology of B16 CTM *in vivo* was similar to 4 T1 CTM (Supporting Information Fig. S1), indicating that the presence of CTM was not tumor-specific. Next, we investigated whether CTM remain hypoxic status *in vivo*. As expected, immunofluorescence staining analysis revealed that 4 T1-mCherry cells in CTM expressed high levels of HIF-1α (Fig. 2C and D), indicating 4 T1 CTM was

undergoing highly hypoxic.

To investigate CTM more conveniently and efficiently, *in vitro* CTM models were established based on the cellular morphology of CTM *in vivo*, which was identified the feature as tumor cell clusters surrounded by platelets inside and NEs outside. By calculating the cell number ratio and keeping the cell viability, we chose the ratios of NEs to tumor cells at 10:1 to simulate CTM *in vitro*, thus the final ratios of 4 T1/B16-mCherry cells to platelets and NEs were 1:800:10. Moreover, we found the vitality of tumor cells hardly declined even at high ratios of NEs (Supporting Information Fig. S2). Then, the morphological features of CTM models were well illuminated by CLSM. 4 T1 CTM and B16 CTM were both formed by tumor cell clusters successively surrounded by platelets and NEs, which was consistent with *in vivo* results (Fig. 2E). In addition, the SEM images also clearly described the status of 4 T1 CTM in tight conjugation (Fig. 2F).

Considering the three-dimensional property during CTM formation process and the close relationship between hypoxia and metastasis [24,25], we speculated that hypoxia may play an important role in CTM mediated metastasis. Western blot analysis was applied and the results showed ~5-fold upregulation of HIF-1α in 4 T1 CTM and ~3-fold upregulation of HIF-1α in B16 CTM *versus* 4 T1 or B16 CL, respectively (Fig. 2G, Supporting Information Fig. S3). To further confirm the results above, elevated level of HIF-1α accumulation was also observed in 4 T1 CTM (Fig. 2H) and the same results were obtained in B16 CTM (Supporting Information Figs. S4 and S5). Moreover, the hypoxia probe was employed to assess whether CTM models remain hypoxia *in vitro*. The results showed that in contrast to 4 T1 CL, more red fluorescent probes were accumulated in 4 T1 CTM, indicating that 4 T1 CTM were highly hypoxic (Fig. 2J). Furthermore, Q-PCR analysis revealed that the downstream genes of HIF-1α including *Glut1*, *Pdk1*, *Vegfa*, *Ldha*, *Gdf15*, *Ccng2*, and *P4ha1* markedly elevated in 4 T1 CTM (Supporting Information Fig. S6). Moreover, EMT related genes *Snail* and *Twist*, which can be promoted by HIF-1α [26], were also increased in CTM (Supporting Information Fig. S7). It has been confirmed that the expression of adhesion molecules is also closely related to the level of HIF-1α [15]. Based on the fact that formation of CTM depends on the interaction of different cells, we then investigated the potential adhesion molecules involved in 4 T1 CTM [27–30]. Q-PCR analysis revealed that four of adhesion molecules genes, including *β3*, *αv*, *P-selectin*, and *Icam-1* were overexpressed in 4 T1 CTM (Supporting Information Fig. S8). It had been reported that P-selectin was the key adhesion molecule that enhanced the interaction between platelet and CTCs [31]. Meanwhile, the elevation of *Icam-1* would further facilitate the recruitment of NEs to CTCs [32]. The above results suggested that upregulation of HIF-1α related adhesion molecules would lead to the formation of CTM. Taken together, these data demonstrated that the simulated CTM *in vitro* remained highly hypoxic and upregulation of HIF-1α accumulation, which was consistent with the situation *in vivo*.

Considering the hypoxic features of CTM, we next investigated the relationship between CTM formation and HIF-1α. $4T1^{HIF\text{-}1\alpha\text{-}KD}$ cells were established and the cluster formation ability was detected. The results showed that clusters formed by $4T1^{HIF\text{-}1\alpha\text{-}KD}$ cells were significantly fewer than 4 T1 cells, indicating knocking down of HIF-1α gene remarkably affected the formation of clusters (Fig. 2I). Moreover, western blot analysis also revealed $4T1^{HIF\text{-}1\alpha\text{-}KD}$ CL could not normally express HIF-1α (Supporting Information Fig. S9) and hypoxia probe staining also illustrated that $4T1^{HIF\text{-}1\alpha\text{-}KD}$ CTM was not hypoxic, even can not form CTM structure (Fig. 2J). Collectively, we infer that HIF-1α is a pivotal element of the CTM formation and there may be a positive feedback loop between the accumulation of HIF-1α with the formation of CTM.

3.2. CTM showed increased metastatic potential

CTM is composed of CTC clusters, platelets and neutrophils, which might play important roles in promoting metastasis. To verify whether CTM have stronger metastatic ability, we prepared different kinds of metastatic entities *in vitro* and directly injected them into tumor-free recipient mice *via* the tail vein (Fig. 3A). The growth of metastases and the overall survival of mice were assayed. As expected, injection of 4 T1-luc CL, 4 T1-luc CL-NEs and 4 T1-luc CL-PLTs resulted in severe tumor metastasis, with mice showing significantly reduced overall survival compared to that of 4 T1-luc single cells (4 T1 SC). Meanwhile, 4 T1 CTM contributing largely to the metastatic burden in the lung and thus representing the most metastatic entity. Interestingly, 4 T1-luc cells that knocked down the HIF-1α gene, either in the forms of single cells ($4T1^{HIF\text{-}1\alpha\text{-}KD}$-luc SC) or clusters ($4T1^{HIF\text{-}1\alpha\text{-}KD}$-luc CL), exhibited the weakest metastatic capacity (Fig. 3B, C and Supporting Information Fig. S10). These results suggested that HIF-1α played a key role in exacerbating metastasis. According to the previous research, intravenous injection of tumor cells is more likely to cause lung metastasis model rather than liver metastasis [33]. Besides, in our study, we also found that although some tumor cells colonize the liver to form liver metastasis, the tumor signal of the lung is much stronger than that of the liver (Fig. 3B). Therefore, our research mainly focuses on lung metastasis.

We then explored the potential mechanism of CTM promoted metastasis. Previous studies reported that PD-L1 is the direct downstream gene of HIF-1α and the high expression of PD-L1 in tumor cells is closely related to immune escape, and played important roles in the process of tumor metastasis [18]. Therefore, we investigated the expression of PD-L1 in 4 T1 CTM by immunofluorescence analysis and found that PD-L1 was highly expressed in 4 T1 CTM *in vivo* (Fig. 3D). *In vitro* study showed that, in comparison to 4 T1 CL, PD-L1 were highly expressed in 4 T1 CTM and majority of the PD-L1 were expressed on the 4 T1 cellular membrane (Fig. 3E). Subsequently, the quantitative expression and distribution of PD-L1 in CTM were confirmed by flow cytometry analysis. Similarly, the results showed the expression of PD-L1 on 4 T1 CL were slightly increased compared with 4 T1 SC, probably ascribed to a certain degree of hypoxia in 4 T1 CL. Meanwhile, PD-L1 was significantly upregulated in 4 T1-NEs and especially in 4 T1 CTM (Fig. 3F, Supporting Information Fig. S11 and Fig. S12). It was worth noting that the expression levels of PD-L1 were extremely low on freshly isolated NEs. However, when incubated with tumor cells, the expression of PD-L1 on NEs was abundantly induced, as demonstrated in 4 T1-NEs and 4 T1 CTM groups (Supporting Information Fig. S12). Thus, the highly expressed PD-L1 on 4 T1 cells and NEs in 4 T1 CTM was consistent with the immunofluorescence results, indicating that CTM was strongly immunosuppressive. HIF-1α can promote EMT program, which has been shown in CTCs [34]. Therefore, we performed immunofluorescence staining of E-cadherin and Vimentin on the sections of lung metastasis. The results showed that the CTM group had high expression of Vimentin and low expression of E-cadherin (Supporting Information Fig. S13), indicating that the tumor cells in CTM had the process of EMT under the influence of HIF-1α.

Taken together, we identified that CTM possessed the great metastasis potential by up regulating PD-L1 and HIF-1α might be the pivotal target for developing effective intervention routines against CTM mediated metastasis.

3.3. Preparation of neutrophil cyto-pharmaceuticals (PNEs)

According to the above results, BAY 87–2243 (BAY) [35], a HIF-1α inhibitor, was applied to further confirmed whether targeted downregulation of HIF-1α in CTM could inhibit CTM mediated metastasis (Fig. 4A). In order to obtain the suitable concentration of BAY for further study, CCK8 assay was conducted and no significant difference was found in cell viability after treatment with BAY up to 20 μM (Supporting Information Fig. S14 and S15). Next, we screened the effective concentration of BAY based on the inhibition of HIF-1α and shrinkage of clusters simultaneously. Western blot analysis showed that HIF-1α accumulation in 4 T1 CL or B16 CL significantly declined with the

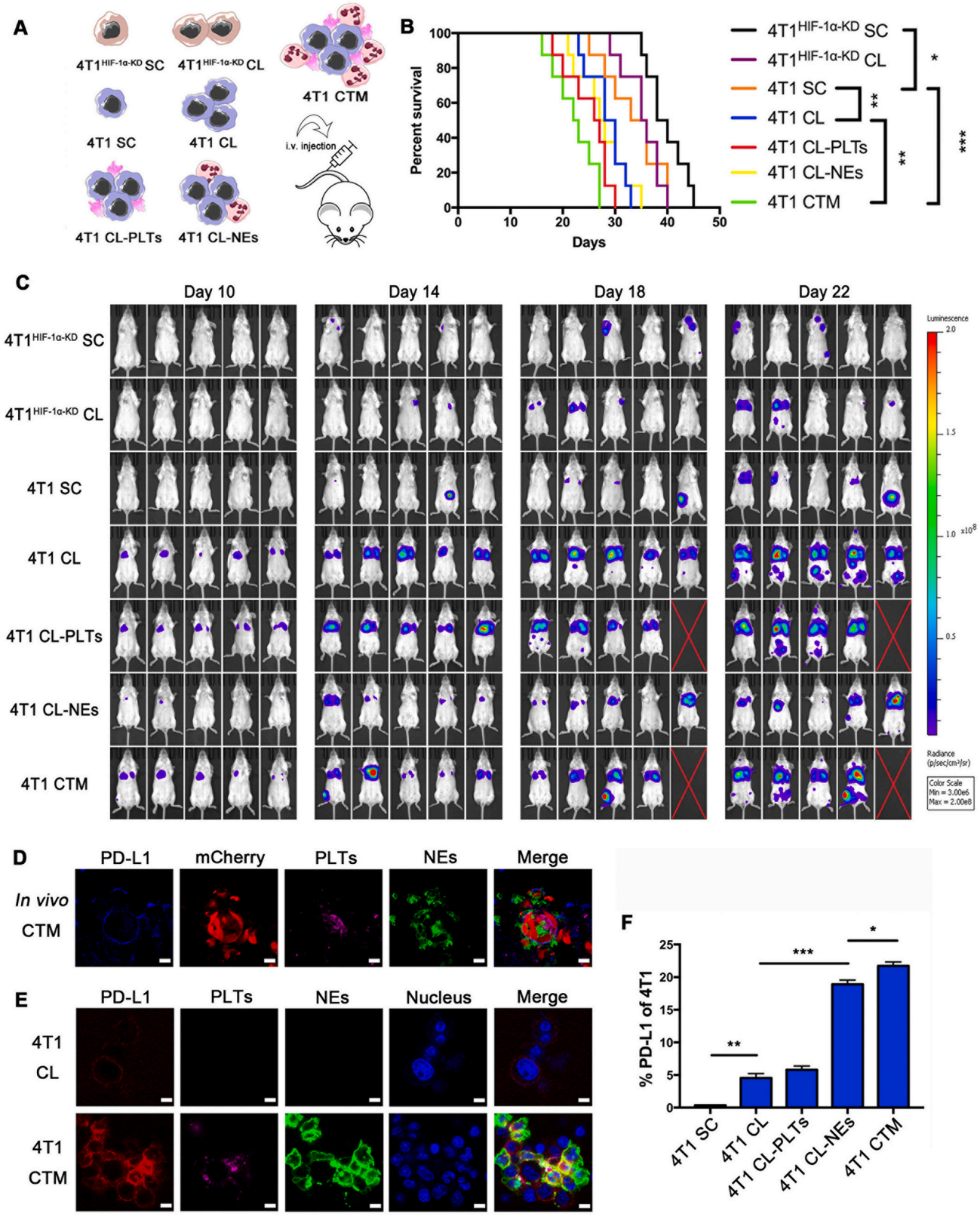

Fig. 3. CTM showed increased metastatic potential. (A) Schematic illustration of the metastatic experimental design of different tumor metastatic entities. (B) Mantel-Cox curve showing percent survival of mice after injection of different tumor metastatic entities. $n = 8$, $^{*}P < 0.05$, $^{**}P < 0.01$, $^{***}P < 0.001$. (C) Representative bioluminescence images of metastasis in mice after tail vein injection of different tumor metastatic entities. $n = 5$. (D) Representative immunofluorescence images of PD-L1 staining (blue) in 4 T1 CL and 4 T1 CTM *in vivo*. 4 T1-mCherry tumor cells (Red) were surrounded by platelets that were labeled with CD41 antibody (Rose red) and neutrophil stained by anti-Ly6G antibody (Green). Scale bar: 5 μm. (E) Representative immunofluorescence images of PD-L1 staining (Red) in 4 T1 CTM *in vitro*. Scale bar: 10 μm. (F) Percent of PD-L1 of 4 T1 cells in different groups. $n = 3$, $^{*}P < 0.05$, $^{**}P < 0.01$. $^{***}P < 0.001$. All experiments were repeated for three time. (For interpretation of the references to colour in this figure legend, the reader is referred to the web version of this article.)

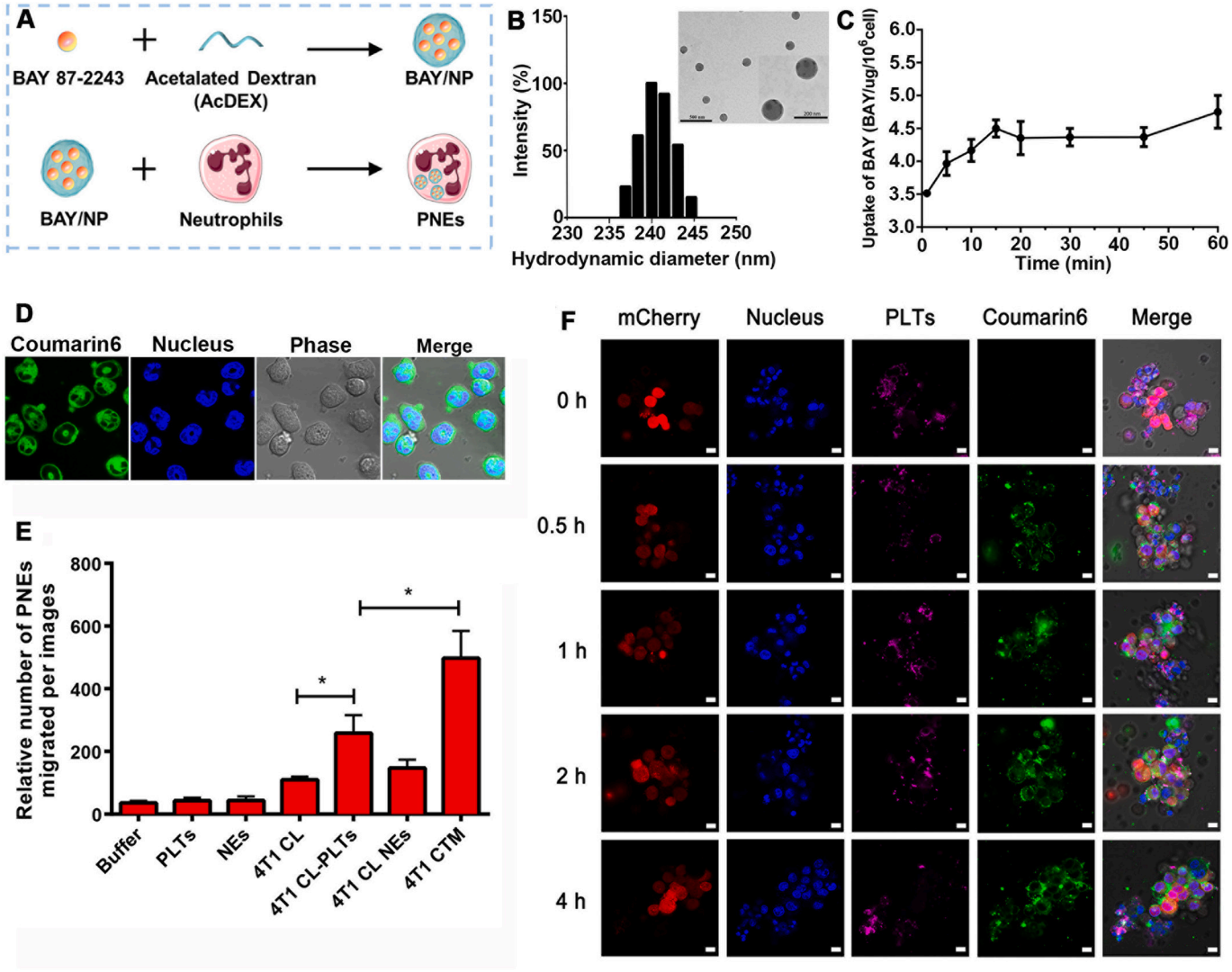

Fig. 4. Preparation of neutrophil cyto-pharmaceuticals (PNEs). (A) Schematic illustration of PNE preparation. (B) The size and SEM image of BAY/NPs. (C) Uptake of BAY87–2243 with different incubation time. (D) The fluorescent image of Coumarin6-tagged PNEs. Scale bar: 5 μm. (E) Relative number of PNEs recruited towards 4 T1 CTM. $n = 12$, $^{*}P < 0.05$, $^{**}P < 0.01$. All experiments were repeated for three times. (F) Time course of coumarin 6 (Green) uptake by 4 T1-mCherry tumor cells (Red) in CTM. Scale bar: 10 μm. (For interpretation of the references to colour in this figure legend, the reader is referred to the web version of this article.)

increase of BAY concentration, and 10 μM had a significant inhibitory effect (Supporting Information Fig. S16 and S17). Moreover, the average size of 4 T1 CL or B16 CL markedly decreased when BAY reached 2 μM and displayed a concentration dependence (Supporting Information Fig. S18 and S19). Taken together, we chose 10 μM as the BAY concentration for the follow-up study.

In order to avoid the side effects of BAY and improve its efficacy, NEs, which could be recruited to CTM *via* chemotaxis [36], were used to construct NE cyto-pharmaceuticals (PNEs) by internalizing BAY loaded acetylated-dextran nanoparticles (BAY/NP). The results showed that BAY could be efficiently loaded into nanoparticles with the particle size about 240 nm when detected by DLS (Fig. 4B). The TEM imaging revealed that BAY/NP was spherical and the particle size was slightly smaller than that of DLS due to the dehydration. To construct PNEs, BAY/NP was simply incubated with NEs and the final PNEs was obtained after centrifugation and washed by PBS to remove unloaded BAY/NP. As shown in Fig. 4C, the internalization of BAY/NP by NEs was time-dependent and achieved plateau after 20 min, which would be used to prepare PNEs for further study. The CLSM assay also revealed that coumarin 6 labeled BAY/NP could be significantly engulfed by NEs (Fig. 4D). After optimization, about 4.3 μg of BAY was found per10^6 PNEs. To investigate whether PNEs exhibit active targeting effect to CTM, we carried out transwell assays to test the chemotaxis of PNEs towards CTM. Intriguingly, we found distinct recruitment of PNEs by 4 T1 CTM or B16 CTM (Fig. 4E, Supporting Information Fig. S20). Meanwhile, there was no significant chemotaxis difference between blank NEs and PNEs (Supporting Information Fig. S21).

Next, we investigated the drug release *in vitro* by simulating the *in vivo* environment, including the normal physiological condition (RPMI medium), during the process of chemotaxis (formyl-met-leu-phe, fMLP), at the site of inflammation (phorbol myristate acetate, PMA) and CTM microenvironment (conditioned medium of CTM). These results showed that PNEs exhibited good stability under physiological condition and during the chemokine chemotaxis process and no drug burst release was found within 8 h. While, PNEs rapidly released the cargoes under the inflammatory microenvironment mimicked by PMA and the conditioned medium of CTM (Supporting Information Fig. S22) after 2 h incubation, indicating that CTM was capable of triggering the release of drug from PNEs.

Additionally, BAY/NP we prepared are positively charged and possesses the function of endo/lysosomal escape the membrane disruption of the cationic lipid of TA_2-Glu-Lys. The function of endo/lysosomal

escape was also investigated and the results showed that BAY/NP could efficiently escape from the endo/lysosome (Supporting Information Fig. S23), which would maintain the stability of BAY/NP intracellularly. Moreover, the intact BAY/NP was also found in the conditional medium (Supporting Information Fig. S24), suggesting that BAY could be deliver to tumor cells in CTM in the form of free drug or BAY/NP. Meanwhile, we also investigated the drug release from BAY/NP with similar condition as described above. The results found that BAY/NP possessed sustained release effect in different media and less 15% of BAY release from BAY/NP after 10 h incubation, which would be benefit to remaining stable within neutrophils and did not damage to cellular function (Supporting Information Fig. S25).

To better understand the drug delivery from PNEs to CTM, coumarin 6 labeled BAY/NP was applied to prepare PNEs (coumarin 6-PNEs). The results showed that when 4 T1 CTM and coumarin 6-PNEs were co cultured for 0.5 h, the accumulation of coumarin 6 in 4 T1-mCherry tumor cells began to increase (Fig. 4F). The uptake process was time-dependently and reached a peak level at 2 h, implying the basis for effective BAY delivery from PNEs towards CTM. Meanwhile, NPs loaded DiD and C6 were applied to investigate the drug release in tumor cells. After the NPs were internalized by tumor cells, the accumulation of DiD and C6 were gradually increased, and changed from colocalization to diffuse in cells (**Supporting Information Fig. S26**). These results suggest that NPs can gradually release drugs in tumor cells. In addition, to better understand the drug release of PNEs *in vivo*, C6 and DiD co-labeled NPs were applied to prepare PNEs, and neutrophils were labeled with DiR. The results showed that when PNEs were injected into the 4 T1 CTM tail vein injection mice, the fluorescence is scattered in lung metastasis, indicating that NPs were separated from neutrophils, and the drugs in NPs were released (**Supporting Information Fig. S27**).

3.4. Intervention effect of PNEs on hypoxia and HIF-1α in CTM

To explore the effect of PNEs on CTM, hypoxia probe staining was applied to assay hypoxic status in CTM. The results showed that 4 T1 CTM visualized apparent hypoxia relief after treatment with BAY, BAY/

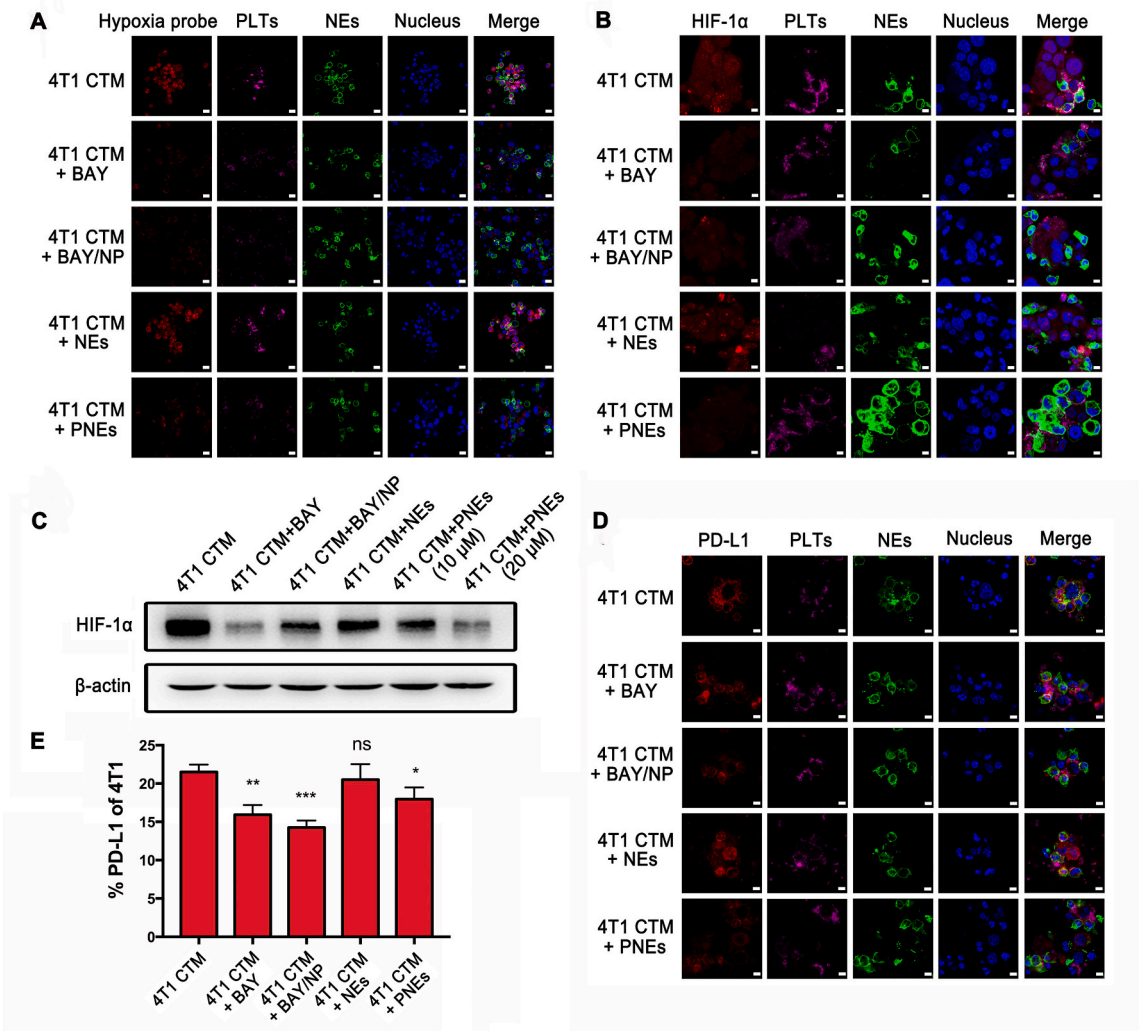

Fig. 5. Intervention of PNEs on hypoxia and HIF-1α in CTM. (A) Representative immunofluorescence images of hypoxia probe staining in 4 T1 CTM after treatment with BAY, BAY/NP, NEs, and PNEs, respectively. 4 T1 tumor cells were surrounded by platelets that were labeled with CD41 antibody (Rose red) and neutrophil stained by anti-Ly6G antibody (Green). Hypoxia probe (Red) in the 4 T1 CTM was evaluated by immunofluorescence. Scale bar: 10 μm. (B) Representative immunofluorescence images of HIF-1α staining in 4 T1 CTM after treatment with BAY, BAY/NP, NEs, and PNEs, respectively. Scale bar: 5 μm. (C) The level of HIF-1α (Red) in 4 T1 CTM after treatment with BAY, BAY/NP, NEs, and PNEs (10 μM and 20 μM) was examined by western blot. Representative gel electrophoresis bands were shown. (D) Representative immunofluorescence images of PD-L1 staining (Red) in 4 T1 CTM after treatment with BAY, BAY/NP, NEs, and PNEs, respectively. Scale bar: 5 μm. (E) Percent of PD-L1 of 4 T1 cells in 4 T1 CTM after treatment with BAY, BAY/NP, NEs, and PNEs, respectively. $n = 3$, ns, not significant, $^{*}P < 0.05$, $^{**}P < 0.01$. $^{***}P < 0.001$. All experiments were repeated for three time. (For interpretation of the references to colour in this figure legend, the reader is referred to the web version of this article.)

NP, and PNEs, whereas no inhibition effect observed with blank NEs (Fig. 5A). The similar results were obtained in B16 CTM (Supporting Information Fig. S28). Then, immunofluorescence staining results confirmed decreased levels of HIF-1α in CTM, which was well consistent with the hypoxia probe results (Fig. 5B, Supporting Information Fig. S29). Furthermore, western blot analysis showed 45% and 53% down-regulation of HIF-1α after PNEs (10 μM) treatment in 4 T1 CTM and B16 CTM, respectively (Fig. 5C, Supporting Information Fig. S30). Additionally, the downstream genes of HIF-1α, such as *Glut1*, *Vegfa*, *Pdk1*, *Ldha*, *Gdf15*, *Ccng2*, and *P4ha1* (Supporting Information Fig. S31),

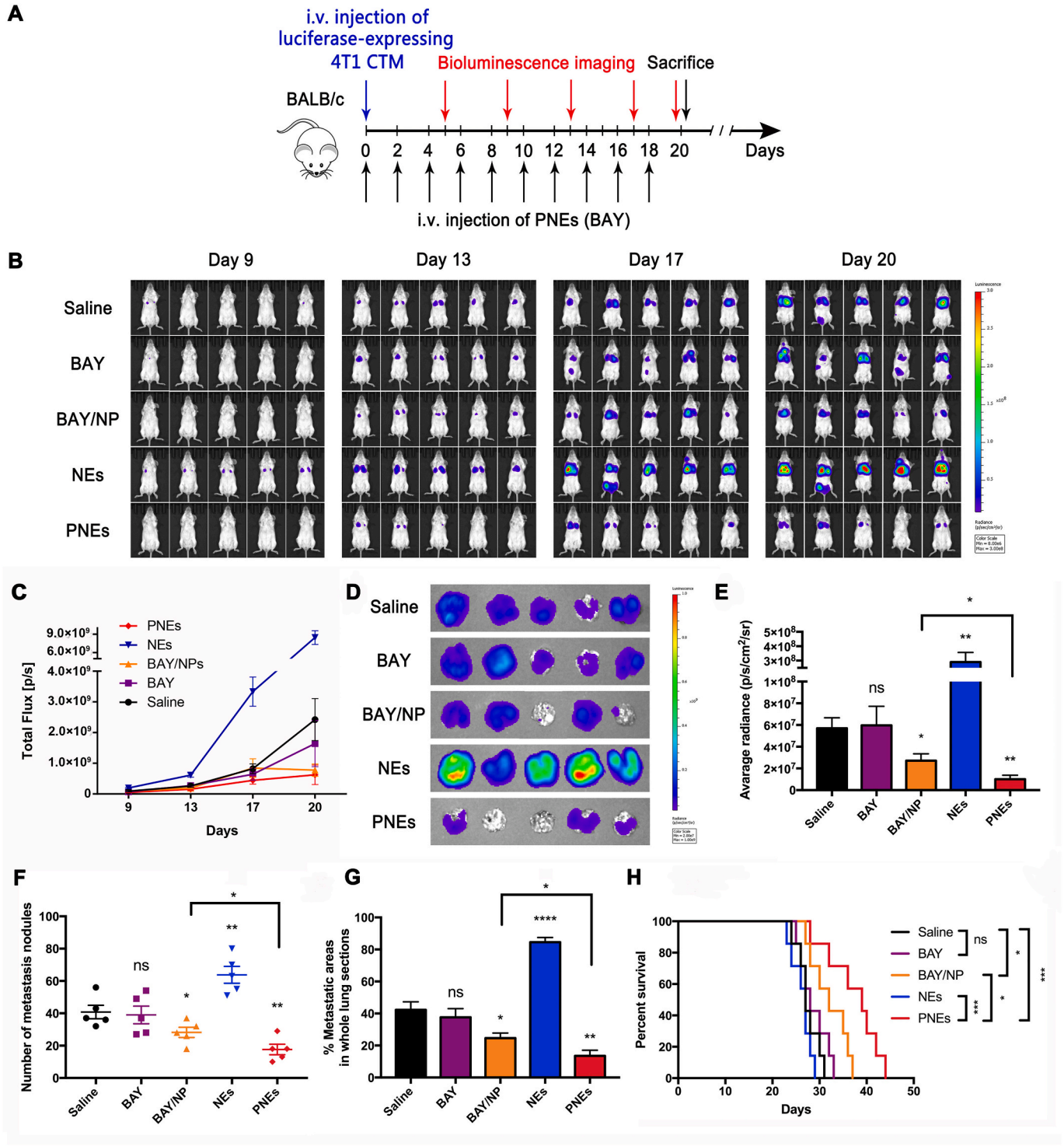

Fig. 6. PNEs effectively inhibited CTM mediated lung metastasis. (A) Schematic illustration of the 4 T1 CTM lung metastasis models establishment and dosing regimen. (B) Bioluminescence images of lung metastasis in 4 T1 CTM tail vein injection mice after treatment of BAY, BAY/NP, NEs, and PNEs. (C) Quantitative analysis of biofluorescence in Fig. 3B. (D) Bioluminescence images of *ex vivo* lungs in different groups. (E) Quantitative analysis of average radiance. $n = 5$, ns, not significant, $^{*}P < 0.05$, $^{**}P < 0.01$. (F) Quantitative analysis of numbers of metastasis nodules in different groups. n = 5, ns, not significant, $^{*}P < 0.05$, $^{**}P < 0.01$. (G) Quantitative analysis of metastatic areas in whole lung sections. n = 5, ns, not significant, $^{*}P < 0.05$, $^{**}P < 0.01$, $^{****}P < 0.0001$. (H) Mantel-Cox curve showing percent survival of mice in different groups. $n = 7$, ns, not significant, $^{*}P < 0.05$, $^{**}P < 0.01$, $^{***}P < 0.001$.

as well as the EMT related genes *Snail* and *Twist* (Supporting Information Fig. S32), which were dramatically elevated in 4 T1 CTM, were all significantly downregulated after treating with PNEs.

Next, we investigated whether the expression of PD-L1 in 4 T1 CTM could be inhibited by PNEs. Immunofluorescence results showed decreased PD-L1 expression after treatment with BAY, BAY/NP, and PNEs, respectively, whereas no obvious difference after treatment with blank NEs (Fig. 5D). Additionally, we analyzed the quantitative expression of PD-L1 on 4 T1 cells and NEs, the results showed that BAY, BAY/NP, and PNEs could significantly inhibit PD-L1 expression on 4 T1 cells (Fig. 5E, Supporting Information Fig. S33). In contrast, the expression of PD-L1 on NEs in each group was hardly affected by different treatments (Supporting Information Fig. S31 and Fig. S34), indicating that the intervention of BAY mainly influenced the expression of PD-L1 on 4 T1 cells, but not on NEs. Collectively, these results demonstrated that PNEs could effectively alleviate hypoxia and downregulate HIF-1α accumulation in CTM. The underlying mechanism of metastasis inhibition by PNEs might be attributed to the downregulation of PD-L1, which would induce the enhanced immune response for inhibiting metastatic tumor cells.

3.5. PNEs effectively inhibited CTM mediated lung metastasis

Based on the active targeting effect of PNEs and the excellent *in vitro* efficacy, we next investigated whether CTM mediated metastasis could be restrained by PNEs. In order to obtain better therapeutic effect, our administration regimen includes early intervention of tumor cells in the circulating emboli and subsequent intervention in the formation period of metastasis. 4 T1 CTM was directly injected into tumor-free recipient mice *via* the tail vein to establish 4 T1 CTM mediated lung metastasis models and mice were treated with PNEs at indicated timepoint (Fig. 6A). The *in vivo* bioluminescence imaging results showed that administration of BAY/NP and PNEs could effectively inhibit the growth of lung metastases (Fig. 6B and C) and quantitative analysis of average radiance of *ex vivo* lungs were consistent with *in vivo* imaging (Fig. 6D and E). Notably, free BAY hardly showed any inhibition effect, probably due to the relatively low concentration of BAY reaching the 4 T1 CTM. Furthermore, mice treated with PNEs had fewer metastatic nodules in lung when compared to that treated with BAY/NP and other groups (Fig. 6F, Supporting Information Fig. S35). Moreover, we analyzed metastatic areas in whole lung sections after PNEs treatment and found the same outcome of minimum area among all groups (Fig. 6G, Supporting Information Fig. S36), indicating that PNEs could maximally inhibit metastases. Correspondingly, mice treated with PNEs survived for the longest time, indicating the superiority of NEs based drug delivery strategy for restraining metastasis (Fig. 6H). Whereas, blank NEs infusion slightly shortened lifespan, probably due to the transformation of NEs into pro-tumor N2 type under the acclimation of tumor cells [37], which cannot be ignored when using PNEs to treat metastasis. In this study, the drug loaded into NEs can reach the target site more effectively, which offsets the problems caused by NEs themselves. In addition, given our previous research, PNEs can prevent extravasation of tumor cells or inhibit the growth of the existing metastasis [38,39]. Therefore, PNEs are still a potential tactics to inhibit CTM mediated metastasis.

Furthermore, the bio-safety study showed that consistent with previous reports, oral administration of BAY resulted in serious gastric erosion and small intestine lesions. However, there was no significant difference between saline and PNEs groups (Supporting Information Fig. S37). Alcian blue staining and quantitative analysis showed typical gastrointestinal toxicity such as loss of crypt cellularity, shortened length of villus and shallowed depth of crypt after BAY administration, while these symptoms were not occurred in PNEs treated mice (Supporting Information Fig. S38), suggesting that PNEs could avoid the side effect of BAY. Additionally, the declining amplitude of body weight of mice remained the mildest in PNEs treatment group (Supporting Information Fig. S39), which further demonstrated the safety and efficacy of PNEs. Collectively, these results confirmed that PNEs could effectively inhibit CTM mediated lung metastasis with good bio-safety.

4. Conclusions

In conclusion, our work confirmed that CTM, which was formed by CTC clusters, platelets and neutrophils, has a high ability to promote tumor metastasis due to hypoxia, upregulation of HIF-1α accumulation and enhanced immune escape. *Via* the chemotaxis of NEs to CTM, we successfully constructed neutrophil cyto-pharmaceuticals loaded with HIF-1α inhibitor (PNEs) for targeted intervening CTM mediated metastasis. Intriguingly, PNEs could significantly relieve hypoxia, downregulate HIF-1α in CTM, finally inhibiting CTM mediated lung metastasis and prolonging the lifespan without side effects. The improved suppression of CTM mediated metastasis by PNEs might be due to the decreased expression of PD-L1, which results in the enhancement of immune response. This study further expands the biological mechanism of tumor metastasis and provides a potential strategy based on neutrophil cyto-pharmaceuticals for treating tumor metastasis.

Author contributions

Junjie Du, Cong Wang, Zhigui Su and Can Zhang designed the research. Junjie Du, Cong Wang, Yijun Chen, Lingyu Zhong, Xuwentai Liu, Lingjing Xue, Ying Zhang, Yanyi Li, Xiaoyu Li, and Chunming Tang performed the experiments. Junjie Du, Cong Wang and Can Zhang analyzed the data. Junjie Du, Cong Wang, and Zhigui Su wrote the manuscript. All of the authors have read and approved the final manuscript.

CRediT authorship contribution statement

Junjie Du: Conceptualization, Writing – original draft, Writing – review & editing, Visualization, Investigation. **Cong Wang:** Methodology, Software, Resources, Data curation, Writing – review & editing, Investigation, Formal analysis. **Yijun Chen:** Writing – original draft, Visualization, Project administration. **Lingyu Zhong:** Investigation. **Xuwentai Liu:** Investigation. **Lingjing Xue:** Investigation. **Ying Zhang:** Investigation. **Yanyi Li:** Investigation. **Xiaoyu Li:** Investigation. **Chunming Tang:** Investigation. **Zhigui Su:** Conceptualization, Visualization, Project administration, Investigation, Writing – review & editing. **Can Zhang:** Conceptualization, Supervision, Project administration, Writing – review & editing.

Declaration of Competing Interest

The authors declare that they have no conflict of interest.

Acknowledgements

We thank the Public Platform of the State Key Laboratory of Natural Medicines for assistance with the pathological-section imaging. This work was supported by the National Natural Science Foundation of China (81930099, 82130102, 81773664, 92159304), the Natural Science Foundation of Jiangsu Province (BK20212011), “Double First-Class” University Project (CPU2018GY47, CPU2018GF10), 111 Project from the Ministry of Education of China and the State Administration of Foreign Expert Affairs of China (No. 111-2-07, B17047), and the Open Project of State Key Laboratory of Natural Medicines (No. SKLNMZZ202017).

Appendix A. Supplementary data

Supplementary data to this article can be found online at https://doi.org/10.1016/j.jconrel.2022.01.051.

References

[1] L. Du, Z. Ning, H. Zhang, F. Liu, Corepressor metastasis-associated protein 3 modulates epithelial-to-mesenchymal transition and metastasis, Chin. J. Cancer 36 (2017) 28, https://doi.org/10.1186/s40880-017-0193-8.

[2] S.C. Williams, Circulating tumor cells, Proc. Natl. Acad. Sci. U. S. A. 110 (2013) 4861, https://doi.org/10.1073/pnas.1304186110.

[3] W. Zhang, F. Wang, C. Hu, Y. Zhou, H. Gao, J. Hu, The progress and perspective of nanoparticle-enabled tumor metastasis treatment, Acta Pharm. Sin. B 10 (2020) 2037–2053, https://doi.org/10.1016/j.apsb.2020.07.013.

[4] S. Gkountela, F. Castro-Giner, B.M. Szczerba, M. Vetter, J. Landin, R. Scherrer, I. Krol, M.C. Scheidmann, C. Beisel, C.U. Stirnimann, C. Kurzeder, V. Heinzelmann-Schwarz, C. Rochlitz, W.P. Weber, N. Aceto, Circulating tumor cell clustering shapes DNA methylation to enable metastasis seeding, Cell 176 (2019) 98–112 e114, https://doi.org/10.1016/j.cell.2018.11.046.

[5] N. Aceto, A. Bardia, D.T. Miyamoto, M.C. Donaldson, B.S. Wittner, J.A. Spencer, M. Yu, A. Pely, A. Engstrom, H.L. Zhu, B.W. Brannigan, R. Kapur, S.L. Stott, T. Shioda, S. Ramaswamy, D.T. Ting, C.P. Lin, M. Toner, D.A. Haber, S. Maheswaran, Circulating tumor cell clusters are oligoclonal precursors of breast cancer metastasis, Cell 158 (2014) 1110–1122, https://doi.org/10.1016/j.cell.2014.07.013.

[6] A.F. Sarioglu, N. Aceto, N. Kojic, M.C. Donaldson, M. Zeinali, B. Hamza, A. Engstrom, H. Zhu, T.K. Sundaresan, D.T. Miyamoto, X. Luo, A. Bardia, B. S. Wittner, S. Ramaswamy, T. Shioda, D.T. Ting, S.L. Stott, R. Kapur, S. Maheswaran, D.A. Haber, M. Toner, A microfluidic device for label-free, physical capture of circulating tumor cell clusters, Nat. Methods 12 (2015) 685–+, https://doi.org/10.1038/Nmeth.3404.

[7] J. Majidpoor, K. Mortezaee, Steps in metastasis: an updated review, Med. Oncol. 38 (2021) 3, https://doi.org/10.1007/s12032-020-01447-w.

[8] F. Gaertner, S. Massberg, Patrolling the vascular borders: platelets in immunity to infection and cancer, Nat. Rev. Immunol. 19 (2019) 747–760, https://doi.org/10.1038/s41577-019-0202-z.

[9] M. Labelle, S. Begum, R.O. Hynes, Platelets guide the formation of early metastatic niches, Proc. Natl. Acad. Sci. U. S. A. 111 (2014) E3053–E3061, https://doi.org/10.1073/pnas.1411082111.

[10] B.M. Szczerba, F. Castro-Giner, M. Vetter, I. Krol, S. Gkountela, J. Landin, M. C. Scheidmann, C. Donato, R. Scherrer, J. Singer, C. Beisel, C. Kurzeder, V. Heinzelmann-Schwarz, C. Rochlitz, W.P. Weber, N. Beerenwinkel, N. Aceto, Neutrophils escort circulating tumour cells to enable cell cycle progression, Nature 566 (2019) 553–557, https://doi.org/10.1038/s41586-019-0915-y.

[11] F. Mollinedo, Neutrophil degranulation, plasticity, and Cancer metastasis, Trends Immunol. 40 (2019) 228–242, https://doi.org/10.1016/j.it.2019.01.006.

[12] C. Donato, L. Kunz, F. Castro-Giner, A. Paasinen-Sohns, K. Strittmatter, B. M. Szczerba, R. Scherrer, N. Di Maggio, W. Heusermann, O. Biehlmaier, C. Beisel, M. Vetter, C. Rochlitz, W.P. Weber, A. Banfi, T. Schroeder, N. Aceto, Hypoxia triggers the Intravasation of clustered circulating tumor cells, Cell Rep. 32 (2020), 108105, https://doi.org/10.1016/j.celrep.2020.108105.

[13] E.B. Rankin, A.J. Giaccia, Hypoxic control of metastasis, Science 352 (2016) 175–180, https://doi.org/10.1126/science.aaf4405.

[14] L. Schito, G.L. Semenza, Hypoxia-inducible factors: master regulators of Cancer progression, Trends Cancer 2 (2016) 758–770, https://doi.org/10.1016/j.trecan.2016.10.016.

[15] Y.P. Tsai, K.J. Wu, Hypoxia-regulated target genes implicated in tumor metastasis, J. Biomed. Sci. 19 (2012) 102, https://doi.org/10.1186/1423-0127-19-102.

[16] M. Labelle, S. Begum, R.O. Hynes, Direct signaling between platelets and cancer cells induces an epithelial-mesenchymal-like transition and promotes metastasis, Cancer Cell 20 (2011) 576–590, https://doi.org/10.1016/j.ccr.2011.09.009.

[17] J. El-Benna, M. Hurtado-Nedelec, V. Marzaioli, J.C. Marie, M.A. Gougerot-Pocidalo, P.M. Dang, Priming of the neutrophil respiratory burst: role in host defense and inflammation, Immunol. Rev. 273 (2016) 180–193, https://doi.org/10.1111/imr.12447.

[18] Q. Gou, C. Dong, H. Xu, B. Khan, J. Jin, Q. Liu, J. Shi, Y. Hou, PD-L1 degradation pathway and immunotherapy for cancer, Cell Death Dis. 11 (2020) 955, https://doi.org/10.1038/s41419-020-03140-2.

[19] F. Basit, L.M. van Oppen, L. Schockel, H.M. Bossenbroek, S.E. van Emst-de Vries, J. C. Hermeling, S. Grefte, C. Kopitz, M. Heroult, P. Hgm Willems, W.J. Koopman, Mitochondrial complex I inhibition triggers a mitophagy-dependent ROS increase leading to necroptosis and ferroptosis in melanoma cells, Cell Death Dis. 8 (2017), e2716, https://doi.org/10.1038/cddis.2017.133.

[20] D. Liu, H. Zhang, E. Makila, J. Fan, B. Herranz-Blanco, C.F. Wang, R. Rosa, A. J. Ribeiro, J. Salonen, J. Hirvonen, H.A. Santos, Microfluidic assisted one-step fabrication of porous silicon@acetalated dextran nanocomposites for precisely controlled combination chemotherapy, Biomaterials 39 (2015) 249–259, https://doi.org/10.1016/j.biomaterials.2014.10.079.

[21] J. Xue, Z. Zhao, L. Zhang, L. Xue, S. Shen, Y. Wen, Z. Wei, L. Wang, L. Kong, H. Sun, Q. Ping, R. Mo, C. Zhang, Neutrophil-mediated anticancer drug delivery for suppression of postoperative malignant glioma recurrence, Nat. Nanotechnol. 12 (2017) 692–700, https://doi.org/10.1038/nnano.2017.54.

[22] A.W. Lambert, D.R. Pattabiraman, R.A. Weinberg, Emerging biological principles of metastasis, Cell 168 (2017) 670–691, https://doi.org/10.1016/j.cell.2016.11.037.

[23] S. Anvari, E. Osei, N. Maftoon, Interactions of platelets with circulating tumor cells contribute to cancer metastasis, Sci. Rep. 11 (2021) 15477, https://doi.org/10.1038/s41598-021-94735-y.

[24] Y. Zhang, H. Zhang, M. Wang, T. Schmid, Z. Xin, L. Kozhuharova, W.K. Yu, Y. Huang, F. Cai, E. Biskup, Hypoxia in breast Cancer-scientific translation to therapeutic and diagnostic clinical applications, Front. Oncol. 11 (2021), 652266, https://doi.org/10.3389/fonc.2021.652266.

[25] J. Yin, H. Cao, H. Wang, K. Sun, Y. Li, Z. Zhang, Phospholipid membrane-decorated deep-penetrated nanocatalase relieve tumor hypoxia to enhance chemo-photodynamic therapy, Acta Pharm. Sin. B 10 (2020) 2246–2257, https://doi.org/10.1016/j.apsb.2020.06.004.

[26] K. Saxena, M.K. Jolly, K. Balamurugan, Hypoxia, partial EMT and collective migration: emerging culprits in metastasis, Transl. Oncol. 13 (2020), 100845, https://doi.org/10.1016/j.tranon.2020.100845.

[27] M. Lavergne, E. Janus-Bell, M. Schaff, C. Gachet, P.H. Mangin, Platelet Integrins in tumor metastasis: do they represent a therapeutic target? Cancers 9 (2017) https://doi.org/10.3390/cancers9100133.

[28] E. Pluskota, N.M. Woody, D. Szpak, C.M. Ballantyne, D.A. Soloviev, D.I. Simon, E. F. Plow, Expression, activation, and function of integrin alphaMbeta2 (Mac-1) on neutrophil-derived microparticles, Blood 112 (2008) 2327–2335, https://doi.org/10.1182/blood-2007-12-127183.

[29] D.J. Wong, D.D. Park, S. Park, C.A. Haller, J. Chen, E. Dai, L. Liu, A.R. Mandhapati, P. Eradi, B. Dhakal, W. Wever, M. Hanes, L. Sun, R.D. Cummings, E.L. Chaikof, A PSGL-1 Glycomimetic reduces Thrombus burden without affecting hemostasis, Blood (2021), https://doi.org/10.1182/blood.2020009428.

[30] G. Steinhoff, M. Behrend, B. Schrader, A.M. Duijvestijn, K. Wonigeit, Expression patterns of leukocyte adhesion ligand molecules on human liver endothelia. Lack of ELAM-1 and CD62 inducibility on sinusoidal endothelia and distinct distribution of VCAM-1, ICAM-1, ICAM-2, and LFA-3, Am. J. Pathol. 142 (1993) 481–488.

[31] L.J. Gay, B. Felding-Habermann, Contribution of platelets to tumour metastasis, Nat. Rev. Cancer 11 (2011) 123–134, https://doi.org/10.1038/nrc3004.

[32] S.J. Huh, S. Liang, A. Sharma, C. Dong, G.P. Robertson, Transiently entrapped circulating tumor cells interact with neutrophils to facilitate lung metastasis development, Cancer Res. 70 (2010) 6071–6082, https://doi.org/10.1158/0008-5472.CAN-09-4442.

[33] B. Weigelt, J.L. Peterse, L.J. Vant Veer, Breast cancer metastasis: markers and models, Nat. Rev. Cancer 5 (2005) 591–602, https://doi.org/10.1038/nrc1670.

[34] Y.F. Sun, W. Guo, Y. Xu, Y.H. Shi, Z.J. Gong, Y. Ji, M. Du, X. Zhang, B. Hu, A. Huang, G.G. Chen, P.B.S. Lai, Y. Cao, S.J. Qiu, J. Zhou, X.R. Yang, J. Fan, Circulating tumor cells from different vascular sites exhibit spatial heterogeneity in epithelial and mesenchymal composition and distinct clinical significance in hepatocellular carcinoma, Clin. Cancer Res. 24 (2018) 547–559, https://doi.org/10.1158/1078-0432.CCR-17-1063.

[35] P. Ellinghaus, I. Heisler, K. Unterschemmann, M. Haerter, H. Beck, S. Greschat, A. Ehrmann, H. Summer, I. Flamme, F. Oehme, K. Thierauch, M. Michels, H. Hess-Stumpp, K. Ziegelbauer, BAY 87-2243, a highly potent and selective inhibitor of hypoxia-induced gene activation has antitumor activities by inhibition of mitochondrial complex I, Cancer Med. 2 (2013) 611–624, https://doi.org/10.1002/cam4.112.

[36] E. Kolaczkowska, P. Kubes, Neutrophil recruitment and function in health and inflammation, Nat. Rev. Immunol. 13 (2013) 159–175, https://doi.org/10.1038/nri3399.

[37] M. Ohms, S. Moller, T. Laskay, An attempt to polarize human neutrophils toward N1 and N2 phenotypes in vitro, Front. Immunol. 11 (2020) 532, https://doi.org/10.3389/fimmu.2020.00532.

[38] Y. Zhang, C. Wang, W. Li, W. Tian, C. Tang, L. Xue, Z. Lin, G. Liu, D. Liu, Y. Zhou, Q. Wang, X. Wang, L. Birnbaumer, Y. Yang, X. Li, C. Ju, C. Zhang, Neutrophil cyto-pharmaceuticals suppressing tumor metastasis via inhibiting hypoxia-inducible factor-1alpha in circulating breast cancer cells, Adv. Healthc. Mat. (2021), e2101761, https://doi.org/10.1002/adhm.202101761.

[39] Y. Li, Q. Hu, W. Li, S. Liu, K. Li, X. Li, J. Du, Z. Yu, C. Wang, C. Zhang, Simultaneous blockage of contextual TGF-beta by cyto-pharmaceuticals to suppress breast cancer metastasis, J. Control. Release 336 (2021) 40–53, https://doi.org/10.1016/j.jconrel.2021.06.012.